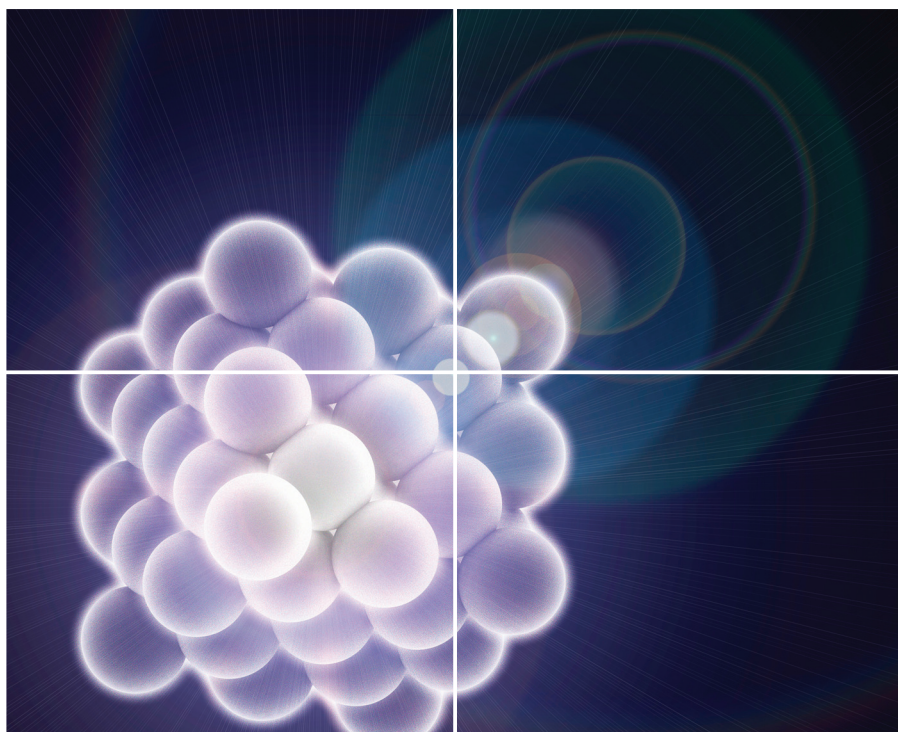


Volume 3 | Number 7 | July 2016



INORGANIC CHEMISTRY

FRONTIERS



<http://rsc.li/frontiers-inorganic>

RESEARCH ARTICLE



Cite this: *Inorg. Chem. Front.*, 2016, **3**, 969

A highly flexible and conductive graphene-wrapped carbon nanofiber membrane for high-performance electrocatalytic applications†

Yunpeng Huang,^a Longsheng Zhang,^a Hengyi Lu,^a Feili Lai,^a Yue-E Miao^{*b} and Tianxi Liu^{*a,b}

The integration of conventional carbonaceous materials with advanced two-dimensional graphene is a challenging but worthwhile attempt to introduce innovative properties into new composites. Herein, we report a novel and facile strategy to create graphene wrapped electrospun carbon nanofiber (GwC) membranes through the surface-induced assembly of graphene oxide (GO) on the surface of pre-oxidized electrospun PAN (oPAN) nanofibers and subsequent carbonization. Driven by the hydrogen bonding between oxygen-containing groups of GO and tertiary amino groups of oPAN, GwC composite membranes with significantly reinforced electrical conductivity are obtained in which every single oPAN fiber is tightly and evenly wrapped by graphene sheets. Additionally, the GwC membrane is further considered as a free-standing template for an *in situ* growth of few-layered MoSe₂ nanosheets. Compared with the graphene-free counterparts, GwC–MoSe₂ composites exhibit a superior electrochemical hydrogen evolution reaction (HER) performance in both acidic and alkaline solutions due to the highly conductive GwC backbone, thus endowing the newly designed GwC membranes with various possibilities for applications in energy-related fields.

Received 22nd April 2016,
Accepted 29th May 2016

DOI: 10.1039/c6qi00101g

rsc.li/frontiers-inorganic

Introduction

Graphene, a single layer sp²-bonded carbon sheet with a hexagonal packed lattice structure, has attracted the most intensive attention since its discovery in 2004.¹ This is mainly due to its genuine advantages over other carbon materials, such as a high Young's modulus (~1 TPa), the quantum hall effect (QHE), high carrier mobility at room temperature (~10 000 cm² V⁻¹ s⁻¹), large theoretical specific surface area (2630 m² g⁻¹), good optical transparency (~97.7%) and excellent thermal conductivity (3000–5000 W m⁻¹ K⁻¹).^{2,3} Such characteristics make graphene and its composites highly desirable for many potential applications in Li-ion batteries,^{4,5} supercapacitors,^{6,7} photovoltaic devices,⁸ sensors,⁹ catalysts,^{10,11} and so on. Particularly, novel electrochemically active

catalysts for a hydrogen evolution reaction (HER) can be synthesized utilizing graphene as a conductive support, attributing to its high surface area and strong electrical coupling effects with other HER active materials, *e.g.* layered transition metal dichalcogenides (LTMD) including MoS₂, MoSe₂, WS₂ and WSe₂.^{12–15} However, most of the graphene-based composites produced *via* hydrothermal reactions, a widely employed hybridizing method, inevitably suffer from easy aggregation and poor dispersion. Besides, the powdery state of conventional graphene-based composites even severely hinders their potential applications in flexible and all-solid-state electronic devices.

Electrospinning is a relatively simple and low-cost strategy to produce continuous polymer nanofibers with a diameter from tens of nanometers to several microns.^{16–19} Carbon nanofiber (CNF) membranes prepared *via* carbonization of the precursor polymer nanofiber membranes,^{20,21} *e.g.* polyacrylonitrile (PAN) and polyimide (PI), have been widely employed in applications such as batteries,^{22–25} electrochemical capacitors,^{26,27} fuel cells,^{28,29} sensors,³⁰ catalysts,^{31,32} and even wearable and portable power sources,^{33,34} owing to their high mechanical strength, electrical conductivity, chemical stability and flexibility. Currently, most of the as-spun PAN nanofibers are stabilized at 250–300 °C in air and carbonized at 600–1100 °C under an inert atmosphere to obtain carbon

^aState Key Laboratory of Molecular Engineering of Polymers, Department of Macromolecular Science, Fudan University, Shanghai, 200433, P. R. China. E-mail: txliu@fudan.edu.cn

^bState Key Laboratory for Modification of Chemical Fibers and Polymer Materials, College of Materials Science and Engineering, Donghua University, Shanghai 201620, P. R. China. E-mail: yuee_miao@dhu.edu.cn

†Electronic supplementary information (ESI) available: Contact angle measurements of PAN and oPAN nanofibrous membranes; SEM images of oPAN nanofibers, CNF–MoSe₂ composites and pure MoSe₂ aggregates. See DOI: 10.1039/c6qi00101g

nanofibers, which are hardly comparable with the commercial ones graphitized at the temperature up to 2800 °C, in consideration of strength and electrical conductivity.³⁵ Excitingly, embedding graphene or carbon nanotubes (CNTs) in electrospun CNFs is greatly beneficial to increase the electrical conductivity.^{36,37} Nevertheless, the improvement is confined to a certain degree due to the limited loading efficiency of incompatible conductive additives in the precursor polymer solutions for stable electrospinning processes.

Herein, a versatile surface-induced assembly method combined with subsequent carbonization is employed for successful fabrication of graphene-wrapped carbon nanofiber (GwC) membranes, in which one-dimensional (1D) CNF is evenly wrapped by two-dimensional (2D) graphene sheets through the hydrogen bonding between graphene oxide and pre-oxidized PAN (oPAN) nanofibers (Scheme 1). The unique combination incorporates the merits of electrically conductive graphene sheets and self-standing electrospun membranes, which largely enhances the conductivity of CNF membranes without sacrificing the high flexibility and mechanical strength, and simultaneously resolves the entanglement and aggregation problems of graphene sheets. Remarkably, a few-layered MoSe₂ nanosheet anchored GwC membrane exhibits superior catalytic activity towards HER with respect to MoSe₂ nanosheets decorated CNF in both acidic and alkaline solutions, demonstrating that graphene-wrapping plays an essential role in improving the electrical conductivity of self-standing GwC membranes.

Experimental

Materials

Polyacrylonitrile (PAN, $M_w = 150\,000\text{ g mol}^{-1}$) was purchased from Sigma-Aldrich. Natural graphite powder (325 meshes) was obtained from Alfa-Aesar. Selenium powder (Se, 99.99%), Na₂MoO₄ (99.99%), hydrazine hydrate (N₂H₄·H₂O, 50 wt% in water), *N,N*-dimethylformamide (DMF), ethanol, 98% H₂SO₄, 30% H₂O₂, KMnO₄, NaNO₃, and 37% HCl were provided by

Sinopharm Chemical Reagent Co. Ltd. All aqueous solutions were prepared with doubly distilled (DI) water.

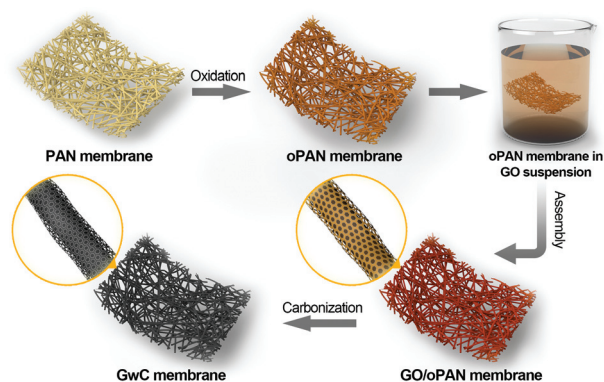
Fabrication of free-standing GwC membranes

The synthesis process of GwC membranes is schematically shown in Scheme 1. PAN nanofibrous membranes with controlled thicknesses were first prepared through a reciprocating single-nozzle electrospinning technique using a commercial electrospinning system (UCALERY Beijing Co., Ltd, China). Typically, a homogeneous solution containing 0.1 g mL⁻¹ PAN was prepared by dissolving PAN powder into DMF under magnetic stirring at 80 °C for 5 h. The freshly obtained precursor solution was then loaded into a 5 mL plastic syringe and injected with a feeding rate of 0.3 mm min⁻¹ through a No. 21 stainless steel needle connected to a high-voltage DC power supply. A rotating aluminum drum was set as the collector with a distance of 15 cm to the needle tip. After 30 min electrospinning under a fixed voltage of 20 kV, PAN nanofibrous membranes were deposited on the aluminum drum. After a 12 h vacuum drying to remove any residual solvents, PAN membranes were then pre-oxidized in air atmosphere at 250 °C for 2 h with a heating rate of 1 °C min⁻¹.

Graphite oxide was synthesized by the Hummers method³⁸ and exfoliated to give a brown dispersion of graphene oxide (GO) under ultrasonication. Then, the tailored oPAN membranes (2 × 3 cm²) were immersed in the GO suspension (2 mg mL⁻¹) at room temperature. After 48 h of soaking to ensure sufficient contact and interactions between GO sheets and oPAN nanofibers, the resulting GO/oPAN membranes were rinsed with absolute ethanol to remove residual GO and water. Finally, the dried GO/oPAN membranes were carbonized in a 900 °C tube furnace for 1 h to yield the self-standing GwC membranes.

Synthesis of GwC-MoSe₂ composites

MoSe₂ nanosheets were grown on GwC membranes *via* a simple solvothermal method according to our previous report.³⁹ Briefly, a 6 mg mL⁻¹ Se solution was first prepared in a flask by adding a certain amount of Se powder into N₂H₄·H₂O. The colorless solution soon turned dark brown after 1 h of magnetic stirring at 80 °C in an oil bath. In a 40 mL teflon-lined autoclave, the vertically placed GwC membrane (10 mg) was immersed in 10 mL of DMF solution containing a stoichiometric amount of Na₂MoO₄. Then, 10 mL of Se solution was added dropwise into the above solution with a final Mo:Se molar ratio of 1:2. Afterwards, the mixture was heated at 180 °C for 12 h to grow MoSe₂ on GwC membranes. After rinsing and drying, the GwC-MoSe₂ composite was annealed in N₂ at 450 °C for 2 h with a ramp rate of 5 °C min⁻¹ to yield a crystallized GwC-MoSe₂ composite. Different concentrations of Se solution (1 mg mL⁻¹, 3 mg mL⁻¹ and 6 mg mL⁻¹) were prepared to adjust the loading amount of MoSe₂, with the corresponding products denoted as GwC-MoSe₂-1, GwC-MoSe₂-3 and GwC-MoSe₂-6, respectively. For comparison, MoSe₂ loaded CNF (denoted as CNF-MoSe₂) membranes and pure MoSe₂ were also produced *via* the above method.



Scheme 1 Schematic illustration of the preparation of GwC nanofibrous membranes.

Characterization

Morphology of the samples was investigated using a field emission scanning electron microscope (FESEM, Zeiss) at an acceleration voltage of 5 kV. Transmission electron microscopy (TEM) was performed under an acceleration voltage of 200 kV with a Tecnai G2 20 TWIN TEM. Fourier transform infrared spectra (FT-IR) were recorded on a Nicolet 6700 FT-IR spectrometer. X-ray diffraction (XRD) experiments were conducted from $2\theta = 10^\circ$ to 80° on an X'Pert Pro X-ray diffractometer with $\text{CuK}\alpha$ radiation ($\lambda = 0.1542$ nm) with a voltage of 40 kV and a current of 40 mA. X-ray photoelectron spectroscopy (XPS) analyses were made with an RBD upgraded PHI-5000C ESCA system (Perkin Elmer) with K (1486.6 eV) as an X-ray source. All XPS spectra were corrected using a C 1s line at 284.6 eV. Curve fitting and background subtraction were accomplished using XPS PEAK41 software. The water contact angles were measured using an automatic video contact-angle testing apparatus (Model OCA 40, Dataphysics). The electrical conductivity of the samples was determined using a Keithley 4200 semi-conductor system at room temperature.

Electrochemical measurements

All electrochemical measurements were conducted with a CHI 660D electrochemical workstation (Chenhua instrument Co., Shanghai, China) at room temperature. The electrochemical HER tests of the GwC-MoSe₂ composite were performed in an electrolyte solution of 0.5 M H₂SO₄ and 1.0 M KOH, respectively. A graphite rod and a saturated calomel electrode (SCE) were used as the counter electrode and the reference electrode, respectively. The working electrode was prepared by pasting a small piece of a GwC-MoSe₂ membrane (3 mm in diameter) onto the polished glassy carbon electrode (GCE) using 5 μL of Nafion solution (5 wt% in ethanol). Pure MoSe₂ modified GCE was prepared *via* dropping 10 μL of MoSe₂ slurry (1 mg mL⁻¹ in DI water) onto GCE and left to dry. Linear sweep voltammetry (LSV) measurements were conducted with a scan rate of 5 mV s⁻¹. In all measurements, the SCE reference electrode was calibrated with respect to the reversible hydrogen electrode (RHE) according to $E(\text{RHE}) = E(\text{SCE}) + 0.281$ V (in 0.5 M H₂SO₄), and $E(\text{RHE}) = E(\text{SCE}) + 1.068$ V (in 1.0 M KOH). Electrochemical impedance spectroscopy (EIS) was recorded in the frequency ranging from 0.01 Hz to 100 kHz at an amplitude of 5 mV under operating conditions (*i.e.*, at a cathodic bias that drives rapid hydrogen evolution) according to the literature,⁴⁰ and in our work the initial electric potential was set as -0.3 V *vs.* RHE for direct comparison. The onset potential was determined based on the beginning of the linear region in the Tafel plot without iR compensation being applied for all the electrochemical measurements.

Results and discussion

Surface-induced assembly of GwC membranes

Pre-oxidized PAN membranes, rather than the as-spun PAN membranes, are intentionally used to prepare GwC mem-

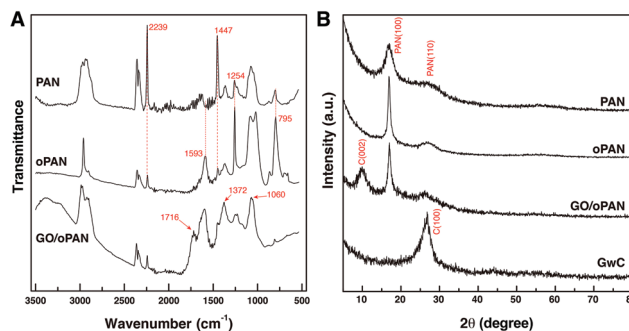


Fig. 1 (A) FTIR spectra of PAN, oPAN and GO/oPAN membranes, (B) XRD curves of PAN, oPAN, GO/oPAN and GwC membranes.

branes based on the considerations that the pre-oxidation process will introduce tertiary amino groups onto oPAN chains, which can efficiently form hydrogen bonds with carboxyl groups and hydroxyl groups on the edge and surface of GO sheets, thus realizing the assembly of GO sheets on oPAN nanofibers. As shown in Fig. S1,[†] the contact angle of the PAN membrane decreases from 117° to 33° after the pre-oxidation treatment, indicating a great improvement in hydrophilicity of the oPAN membrane. To yield a high-strength and stable CNF membrane, pre-oxidation is also indispensable to convert the linear PAN chains into aromatic ladder structures, thus rendering oPAN nanofibers with non-meltable characteristics to be prevented from fusing together during carbonization.³⁵ As shown in Fig. 1A, two characteristic peaks at 2239 and 1447 cm^{-1} are attributed to the $\text{C}\equiv\text{N}$ stretching vibration and $\text{C}-\text{N}$ stretching vibration of PAN according to previous reports.⁴¹ The intensity of both peaks decreases sharply after pre-oxidation due to the cyclization and dehydrogenation of PAN during heat treatment. No peaks can be observed at $3000\text{--}3500\text{ cm}^{-1}$, excluding the existence of primary or secondary amino groups in oPAN. Besides, three new peaks at 1593, 1254 and 995 cm^{-1} emerge in the curve of oPAN, which can be assigned to the $\text{C}=\text{N}$, $\text{C}-\text{C}$ and $\text{C}-\text{N}$ stretching vibrations, and a $\text{C}-\text{H}$ out-of-plane wagging vibration, respectively, confirming the introduction of tertiary amino groups into oPAN during the pre-oxidation reaction.

The existence of interconnected macroporous structures within the oPAN nanofibrous membrane (Fig. S2[†]) is highly desirable for the infiltration and diffusion of GO sheets in an aqueous medium, which would benefit the uniform assembly of GO on oPAN nanofibers. The FTIR spectrum of the GO/oPAN membrane indicates the presence of $\text{C}-\text{O}$ (1060 cm^{-1}), $\text{C}-\text{OH}$ (1226 cm^{-1}) and $\text{C}=\text{O}$ (1716 cm^{-1}) groups of GO (Fig. 1A).⁴² The XRD curve (Fig. 1B) of the GO/oPAN membrane confirms the existence of a C(002) peak of GO, while the other two peaks at $2\theta = 17^\circ$ and 29.5° are assigned to the improved crystallite structure of oPAN after pre-oxidation. Furthermore, the C(100) peak occurs at $2\theta = 27^\circ$ (Fig. 1B) when the GO/oPAN membrane is finally carbonized into GwC at 900°C , with oPAN nanofibers converted into carbon nanofibers while GO is simultaneously reduced to form reduced graphene oxide

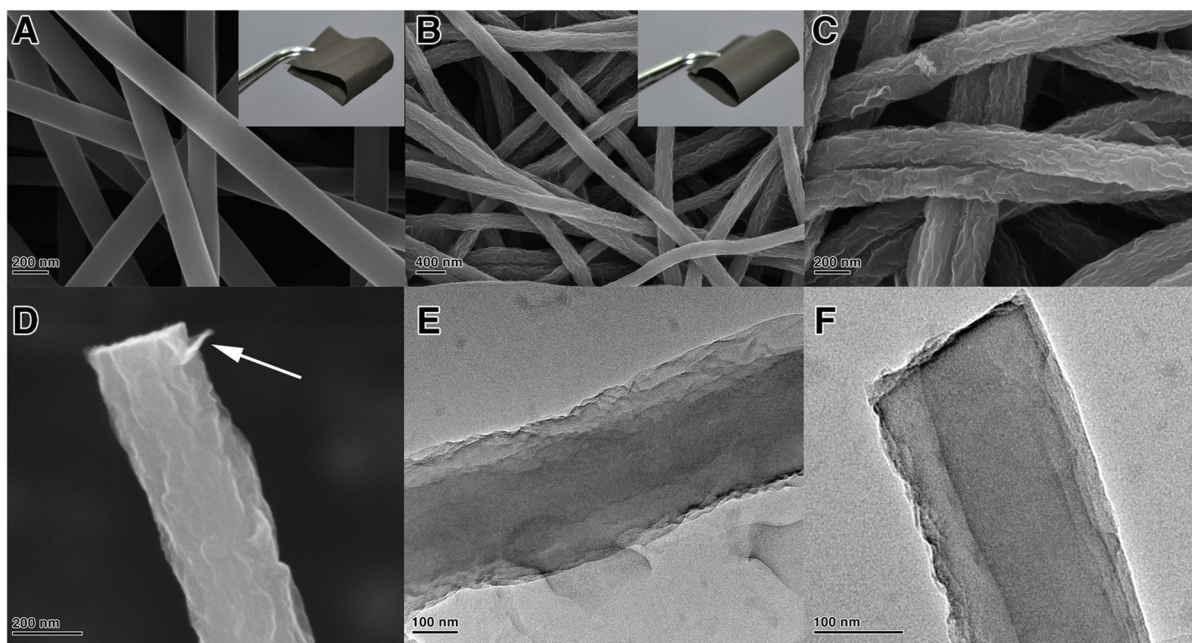


Fig. 2 FESEM images of (A) bare CNF, and (B–D) GwC membranes under different magnifications. (E and F) TEM images of the GwC membrane showing the effective wrapping of graphene on the surface of CNF. The insets of (A and B) demonstrate the flexibility of both bare CNF and GwC membranes.

(hereinafter referred to as graphene). Interestingly, a sharp contrast can be observed in Fig. 2A and B that the smooth surface of CNF nanofibers becomes rough and irregular after the assembly of graphene sheets. A zoom-in observation in Fig. 2C reveals the unique configuration of graphene-wrapped carbon nanofibers, confirming that every single fiber is evenly wrapped by corrugated graphene sheets. The cross section of one single fiber shows that graphene sheets are peeled off during the fracture process (as indicated by the white arrow in Fig. 2D), indicating the successful wrapping of graphene on carbon nanofibers. It is also obvious that the flexibility of CNF is perfectly retained by the GwC membrane (insets of Fig. 2A and B). TEM images in Fig. 2E and F further reveal the novel structure of GwC, confirming that one carbon nanofiber is enveloped by multiple layers of graphene sheets. The tightly wrapped graphene layers serving as the conductive casing will definitely improve the electrical conductivity of the carbon nanofibers.

The cross-section SEM images of the GwC membrane are provided in Fig. 3 to further probe the distribution of graphene along the Z-axis of the GwC membrane. The thickness of the self-standing GwC membrane is about 45 μm (Fig. 3A). High-resolution SEM images (Fig. 3B–D) focused on different regions (marked by red rectangles in Fig. 3A) indicate that graphene sheets are uniformly distributed in full depth along the Z-axis of the GwC membrane, confirming that GO sheets are able to diffuse throughout the oPAN membrane by virtue of the interconnected pores of electrospun nanofiber membranes. All these pieces of evidence indicate the successful wrapping of graphene on electrospun CNF membranes and

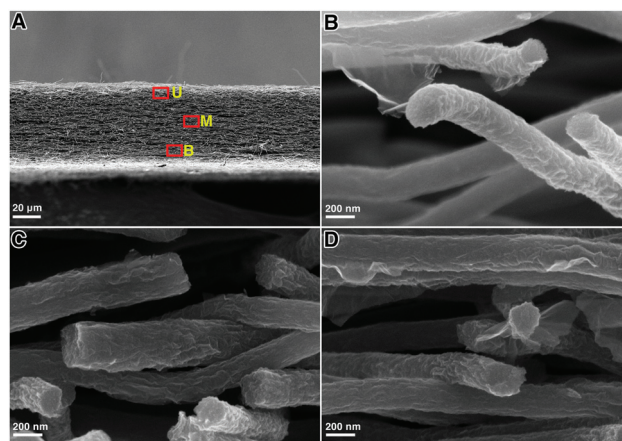
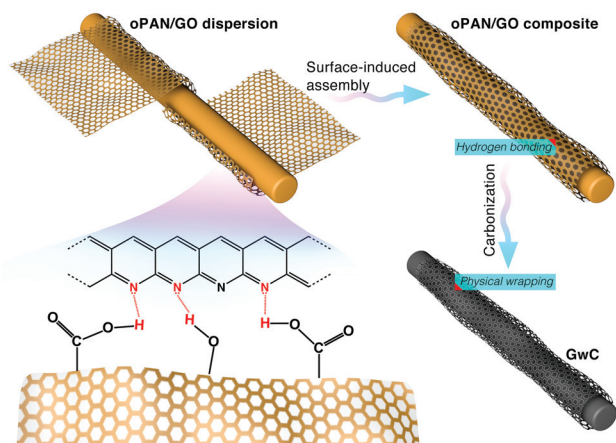


Fig. 3 (A) Cross-sectional image of the GwC nanofibrous membrane and the corresponding magnified images from (B) upper region U, (C) middle region M, and (D) bottom region B.

highlight the feasibility of our protocol to integrate low-dimensional carbonaceous materials together.

Based on the above characterization, a two-step surface-induced assembly process is proposed in the preparation of GwC (Scheme 2). In the first step, GO sheets penetrate into the oPAN nanofiber network in an aqueous medium and interact with oPAN fibers through hydrogen bonds between the oxygen-containing groups on GO and tertiary amino groups on oPAN, thus resulting in the surface-induced assembly of GO sheets till the interaction becomes too weak to support the process. Thus the obtained GO-wrapped oPAN nanofibers are



Scheme 2 Schematic illustration showing the two-step assembly processes during the preparation of GwC membrane.

subsequently treated at a high temperature to yield GwC membranes, with the hydrogen-bonded GO sheets synchronously converted to physically wrapped graphene.

Structure of GwC–MoSe₂ composites

The GwC membranes can be used as self-standing substrates for the immobilization of various electrochemically active materials owing to their porosity, large surface area and operability. Hence, a facile low-temperature solvothermal process combined with post annealing treatment was utilized to deposit crystalline MoSe₂ nanosheets on GwC membranes. As shown in Fig. 4A, only a few inconspicuous MoSe₂ whiskers are scattered on the surface of GwC fibers under low Se

dosage. For GwC–MoSe₂-3 composites (Fig. 4B and C), MoSe₂ subunits with a curled shape and perpendicular orientation are evenly distributed on the surfaces of graphene-wrapped carbon nanofibers, which also interconnect with each other to form a unique open network architecture. This can provide numerous exposed active edges and fast pathways for ion and electron transfer, thus potentially leading to an enhanced electrocatalytic activity. Further increasing the Se concentration to 6 mg mL⁻¹ (Fig. 4D), MoSe₂ nanosheets tend to agglomerate and block the porous structure of the GwC membrane, which deteriorates the overall electrochemical performance. The TEM image in Fig. 4E shows a well-defined core-shell structure of the GwC–MoSe₂-3 composite. The high-resolution TEM image (Fig. 4F) indicates that MoSe₂ nanosheets in the composite are composed of multiple MoSe₂ single layers with the interlayer spacing of 0.65 nm, in good accordance with the (002) lattice spacing of MoSe₂. All these morphological characterization methods give a visual confirmation on the successful synthesis of few-layered MoSe₂ nanosheets on GwC membranes. A MoSe₂ decorated CNF membrane was also prepared (with the absence of graphene wrapping) under the same Se concentration as the GwC–MoSe₂-3 composite, which shows an identical morphology as shown in Fig. S3.†

The crystal structure of the GwC–MoSe₂-3 composite was studied using XRD as shown in Fig. 5A. The diffraction peaks at $2\theta = 13.7^\circ, 26.4^\circ, 32.2^\circ, 37.3^\circ, 54.1^\circ$ and 56.6° can be respectively indexed to the (002), (004), (100), (103), (106) and (008) diffraction planes of the hexagonal 2H–MoSe₂ phase (JCPDF card, no. 87-2419), revealing the high crystallinity of few-layered MoSe₂ nanosheets on GwC. XPS analysis was conducted to further analyze the chemical composition and

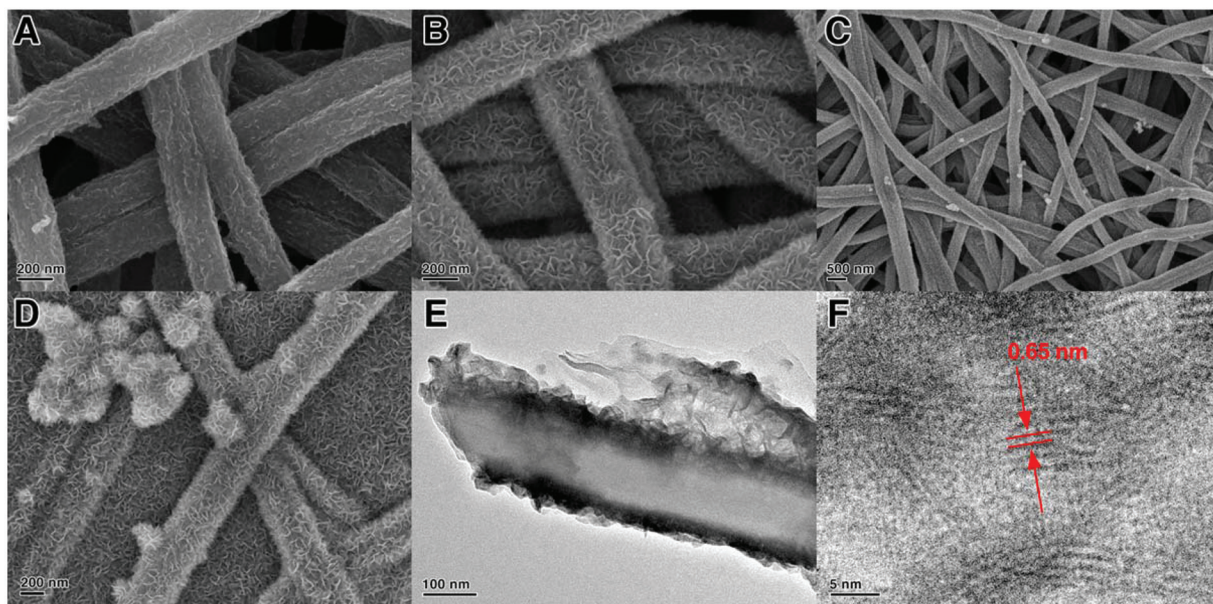


Fig. 4 FESEM images of (A) GwC–MoSe₂-1, (B and C) GwC–MoSe₂-3, (D) GwC–MoSe₂-6 composites. (E and F) TEM images of GwC–MoSe₂-3 composite under different magnifications.

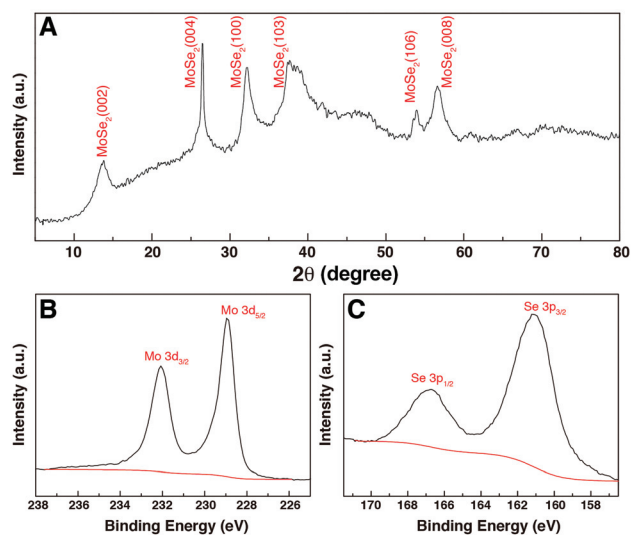


Fig. 5 (A) XRD pattern and (B and C) XPS spectra of GwC-MoSe₂-3 composite.

valence states of the GwC-MoSe₂-3 composite. As shown in Fig. 5B, the high-resolution spectrum of Mo 3d exhibits two peaks at 228.9 and 232.1 eV assigned to Mo 3d_{5/2} and Mo 3d_{3/2} orbitals, respectively, confirming the formation of Mo⁴⁺. Binding energies of Se 3p_{3/2} and Se 3p_{1/2} at 160.8 and 166.6 eV indicate the chemical oxidation state of Se²⁻ (Fig. 5C). Additionally, a detailed compositional analysis reveals that the surface atomic ratio of Mo:Se is 10:22, which is close to the formula of MoSe₂.

Electrochemical evaluation of HER catalyst

The electrocatalytic HER activity of the GwC-MoSe₂ composite modified GCE was first investigated in an acidic medium of 0.5 M H₂SO₄ solution using a typical three-electrode setup. As shown in Fig. 6A, Pt exhibits an extremely high HER catalytic activity with a near zero onset potential and a large current density. In contrast, the bare GwC membrane modified GCE shows almost no HER activity with a near flat line within the potential window. Pure MoSe₂ exhibits a noteworthy HER activity owing to the intrinsic electrocatalytic activity of LTMD, but with a much lower anodic current and a more negative onset potential (−0.16 V vs. RHE) compared with those of GwC-MoSe₂ composites, which is ascribed to the intrinsic low electrical conductivity and severely decreased active sites of agglomerated MoSe₂ spheres (Fig. S4†). The GwC-MoSe₂-1 composite shows obviously enhanced HER activity even with a minor MoSe₂ loading, indicating the essential role of the GwC membrane as an advanced catalyst support. For the GwC-MoSe₂-3 composite modified electrode, the LSV curve shows greatly improved current intensity and more positive onset potential of −0.08 V vs. RHE, which outperforms most of the previously reported MoS₂- or MoSe₂-based HER catalysts including exfoliated MoS₂ nanosheets (−0.12 V),⁴³ few-layered MoS₂ nanosheets obtained by the chemical vapor deposition method (−0.15 V),⁴⁴ and S-doped MoSe₂ nanosheets (−0.1 V)⁴⁵. However, the HER activity of GwC-MoSe₂-3 is still inferior to that (−0.05 V) of the MoSe₂/graphene hybrid due to its higher electrical conductivity of a pure graphene support.⁴⁶ With respect to the GwC-MoSe₂-6 composite modified GCE, the LSV curve negatively shifts with decreased activity. Possible reasons for the different HER electrocatalytic activities can be

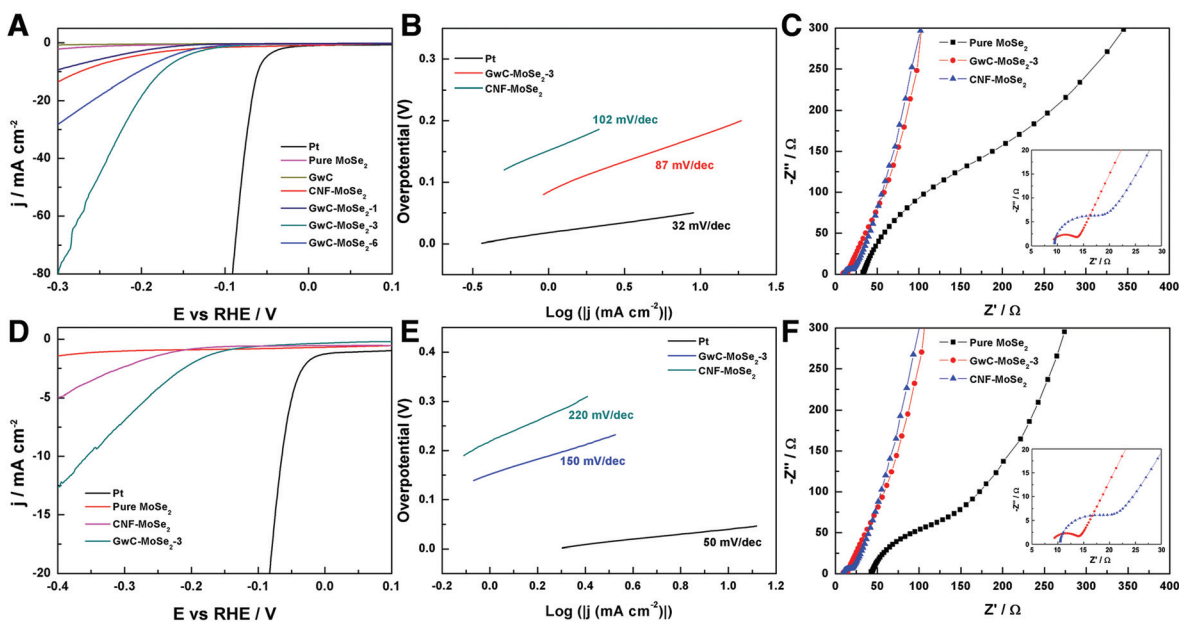


Fig. 6 Electrochemical HER activity tests on different sample modified GCEs in (A–C) 0.5 M H₂SO₄ and (D–F) 1.0 M KOH: (A and D) LSV polarization curves for Pt, pure MoSe₂ spheres, GwC, GwC-MoSe₂ and CNF-MoSe₂ composites, (B and E) the corresponding Tafel plots, and (C and F) EIS spectra of pure MoSe₂ spheres, GwC-MoSe₂-3 and CNF-MoSe₂ composites.

concluded from the morphological difference as shown in Fig. 3A–C. The GwC–MoSe₂-3 composite shows an optimized hierarchical structure with a more uniform distribution of MoSe₂ nanosheets and more exposed active edges compared with the GwC–MoSe₂-1 and GwC–MoSe₂-6 composites, which can provide more reaction sites for the HER process and facilitate fast ion/electron transfer, thus leading to better HER catalytic activity. Moreover, the CNF–MoSe₂ composite exhibits inferior HER performance in terms of low current intensity and negatively shifted onset potential (−0.12 V *vs.* RHE) with respect to GwC–MoSe₂-3 composites, further confirming the great importance of graphene wrapping in the enhancement of electrochemical behavior.

The corresponding Tafel plots in Fig. 6B show that the Tafel slopes for Pt, GwC–MoSe₂-3 and CNF–MoSe₂ composites are 32, 87 and 102 mV per decade, respectively (obtained from the Tafel equation $\eta = b \log(j) + a$, where η is the overpotential, j is the current density and b is the Tafel slope). The small Tafel slope of the GwC–MoSe₂-3 composite indicates a faster increase of the HER rate with increasing overpotential, which is favorable for practical applications. EIS measurements for pure MoSe₂, GwC–MoSe₂-3 and CNF–MoSe₂ composites are performed to understand their electrochemical behavior during the HER process. As shown in Fig. 6C, both the charge transfer resistance (R_{ct} , the visible semicircles in high frequency region) and series resistance (R_s , the x -intercept of Nyquist plots) of MoSe₂ decrease dramatically after growing on CNF and GwC membranes, indicating that both CNF and GwC nanofibrous supports can serve as conductive backbones to accelerate the ion diffusion and charge transfer. Additionally, the enlarged high frequency region in the inset of Fig. 6C reveals a smaller R_{ct} of the GwC–MoSe₂-3 composite with respect to the CNF–MoSe₂ composite, demonstrating that the wrapped graphene layers can largely improve the electrical conductivity (12.90 S m^{−1}) of the GwC membrane compared with that (0.39 S m^{−1}) of the CNF membrane.

Furthermore, the HER performance of the GwC–MoSe₂-3 composite is also evaluated under alkaline conditions. As shown in Fig. 6D and E, GwC–MoSe₂-3 modified GCE shows the best alkaline HER activity with an onset potential of −0.138 V *vs.* RHE and a Tafel slope of 150 mV per decade compared with pure MoSe₂ (onset potential of \sim −0.3 V *vs.* RHE) and the CNF–MoSe₂ composite (onset potential of −0.19 V *vs.* RHE and a Tafel slope of 220 mV per decade), which is also comparable to the behaviors of most reported advanced HER catalysts in basic media, such as bulk MoB,⁴⁷ Co-embedded nitrogen-rich carbon nanotubes (CNTs),⁴⁸ and CoP coated carbon cloth.⁴⁹ The EIS results under alkaline conditions are identical to those in acidic media, despite the R_{ct} of the GwC–MoSe₂-3 electrode slightly increasing, implying better HER performance of GwC–MoSe₂-3 in an acidic medium. To assess the stability of the GwC–MoSe₂-3 composite during the HER process, time-dependent current density curves were respectively collected under acidic and alkaline conditions for 5000 s at the static overpotentials (−0.16 V in 0.5 M H₂SO₄, and −0.28

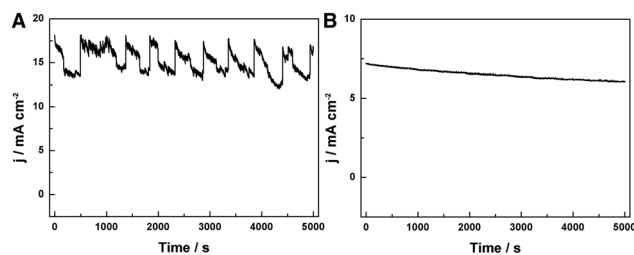


Fig. 7 Time-dependent current density curves at static overpotentials of (A) −0.16 V in 0.5 M H₂SO₄ and (B) −0.28 V in 1.0 M KOH, respectively.

V in 1 M KOH) (Fig. 7A and B), both of which demonstrate excellent long-term stability of the GwC–MoSe₂-3 electrode at a constant high current density. The remarkable electrochemical HER performance of the GwC–MoSe₂-3 composite is attributed to the synergistic effects between graphene reinforced CNF and HER active MoSe₂ nanosheets. The GwC membrane can direct the uniform distribution of MoSe₂ and offer conductive networks for a fast charge transfer while perpendicularly oriented few-layered MoSe₂ nanosheets with numerous exposed active edges provide sufficient electrochemical sites for efficient HER reaction. This electrochemical evidence further highlight the novel design of this fascinating GwC composite membrane as an electrically reinforced catalyst support, which is envisioned to be applied in the fabrication of various energy-related devices including supercapacitors, fuel cells, Li-ion batteries, *etc.*

Conclusions

In summary, we have developed a versatile and additive-free hydrogen bonding directed assembly approach for the uniform wrapping of graphene sheets on electrospun carbon nanofibers to obtain a GwC composite. By combining the advantages of both carbonaceous materials, the GwC composite membrane demonstrates to be a superior catalyst support for electrochemical HER. Surprisingly, the as-obtained GwC–MoSe₂ composites exhibit greatly enhanced electrochemical HER performance in both acidic and alkaline solutions with respect to the MoSe₂ anchored CNF composite, which is mainly ascribed to the improved electrical conductivity of GwC and evenly distributed few-layered MoSe₂ nanosheets. Furthermore, such a facile surface-induced assembly strategy opens a new avenue for the reconstruction of conventional electrospun CNF membranes towards high-performance energy storage and conversion applications.

Acknowledgements

The authors are grateful for the financial support from the National Natural Science Foundation of China (51125011, 51373037, 51433001).

Notes and references

- 1 K. S. Novoselov, A. K. Geim, S. V. Morozov, D. Jiang, Y. Zhang, S. V. Dubonos, I. V. Grigorieva and A. A. Firsov, *Science*, 2004, **306**, 666–669.
- 2 C. G. Lee, X. D. Wei, J. W. Kysar and J. Hone, *Science*, 2008, **321**, 385–388.
- 3 R. R. Nair, P. Blake, A. N. Grigorenko, K. S. Novoselov, T. J. Booth, T. Stauber, N. M. R. Peres and A. K. Geim, *Science*, 2008, **320**, 1308–1308.
- 4 Y. J. Gong, S. B. Yang, Z. Liu, L. L. Ma, R. Vajtai and P. M. Ajayan, *Adv. Mater.*, 2013, **25**, 3979–3984.
- 5 D. B. Kong, H. Y. He, Q. Song, B. Wang, W. Lv, Q. H. Yang and L. J. Zhi, *Energy Environ. Sci.*, 2014, **7**, 3320–3325.
- 6 G. Z. Sun, J. Q. Liu, X. Zhang, X. W. Wang, H. Li, Y. Yu, W. Huang, H. Zhang and P. Chen, *Angew. Chem., Int. Ed.*, 2014, **53**, 12576–12580.
- 7 H. Xia, C. Hong, B. Li, B. Zhao, Z. X. Lin, M. B. Zheng, S. V. Savilov and S. M. Aldoshin, *Adv. Funct. Mater.*, 2015, **25**, 627–635.
- 8 Z. Y. Yin, S. X. Wu, X. Z. Zhou, X. Huang, Q. C. Zhang, F. Boey and H. Zhang, *Small*, 2010, **6**, 307–312.
- 9 H. X. Chang, L. H. Tang, Y. Wang, J. H. Jiang and J. H. Li, *Anal. Chem.*, 2010, **82**, 2341–2346.
- 10 M. R. Gao, X. Cao, Q. Gao, Y. F. Xu, Y. R. Zheng, J. Jiang and S. H. Yu, *ACS Nano*, 2014, **8**, 3970–3978.
- 11 D. U. Lee, B. J. Kim and Z. W. Chen, *J. Mater. Chem. A*, 2013, **1**, 4754–4762.
- 12 J. J. Duan, S. Chen, B. A. Chambers, G. G. Andersson and S. Z. Qiao, *Adv. Mater.*, 2015, **27**, 4234–4241.
- 13 L. P. Jia, X. Sun, Y. M. Jiang, S. J. Yu and C. M. Wang, *Adv. Funct. Mater.*, 2015, **25**, 1814–1820.
- 14 Y. G. Li, H. L. Wang, L. M. Xie, Y. Y. Liang, G. S. Hong and H. J. Dai, *J. Am. Chem. Soc.*, 2011, **133**, 7296–7299.
- 15 Y. P. Huang, H. Y. Lu, H. H. Gu, J. Fu, S. Y. Mo, C. Wei, Y. E. Miao and T. X. Liu, *Nanoscale*, 2015, **7**, 18595–18602.
- 16 M. Bazhban, M. Nouri and J. Mokhtari, *Chin. J. Polym. Sci.*, 2013, **31**, 1343–1351.
- 17 A. Greiner and J. H. Wendorff, *Angew. Chem., Int. Ed.*, 2007, **46**, 5670–5703.
- 18 D. Li and Y. N. Xia, *Adv. Mater.*, 2004, **16**, 1151–1170.
- 19 Z. Y. Xiong, X. Y. Kong, Z. X. Guo and J. Yu, *Chin. J. Polym. Sci.*, 2015, **33**, 1234–1244.
- 20 M. Inagaki, Y. Yang and F. Kang, *Adv. Mater.*, 2012, **24**, 2547–2566.
- 21 Z. Y. Zhang, X. H. Li, C. H. Wang, S. W. Fu, Y. C. Liu and C. L. Shao, *Macromol. Mater. Eng.*, 2009, **294**, 673–678.
- 22 Y. E. Miao, Y. P. Huang, L. S. Zhang, W. Fan, F. L. Lai and T. X. Liu, *Nanoscale*, 2015, **25**, 11093–11101.
- 23 Y. Z. Wu, M. V. Reddy, B. V. R. Chowdari and S. Ramakrishna, *ACS Appl. Mater. Interfaces*, 2013, **5**, 12175–12184.
- 24 G. J. Wei, M. H. Jing, X. Z. Fan, J. G. Liu and C. W. Yan, *J. Power Sources*, 2015, **287**, 81–86.
- 25 C. Flox, C. Fabrega, T. Andreu, A. Morata, M. Skoumal, J. Rubio-Garcia and J. R. Morante, *RSC Adv.*, 2013, **3**, 12056–12059.
- 26 A. Ghosh, E. J. Ra, M. H. Jin, H. K. Jeong, T. H. Kim, C. Biswas and Y. H. Lee, *Adv. Funct. Mater.*, 2011, **21**, 2541–2547.
- 27 X. Li, X. B. Zang, Z. Li, X. M. Li, P. X. Li, P. Z. Sun, X. Lee, R. J. Zhang, Z. H. Huang, K. L. Wang, D. H. Wu, F. Y. Kang and H. W. Zhu, *Adv. Funct. Mater.*, 2013, **23**, 4862–4869.
- 28 M. Y. Li, G. Y. Han and B. S. Yang, *Electrochem. Commun.*, 2008, **10**, 880–883.
- 29 J. H. Park, Y. W. Ju, S. H. Park, H. R. Jung, K. S. Yang and W. J. Lee, *J. Appl. Electrochem.*, 2009, **39**, 1229–1236.
- 30 Y. P. Huang, Y. E. Miao, S. S. Ji, W. W. Tjiu and T. X. Liu, *ACS Appl. Mater. Interfaces*, 2014, **6**, 12449–12456.
- 31 S. G. Wang, Z. T. Cui and M. H. Cao, *Chem. – Eur. J.*, 2015, **21**, 2165–2172.
- 32 W. X. Yang, Y. Q. Zhang, C. Y. Liu and J. B. Jia, *J. Power Sources*, 2015, **274**, 595–603.
- 33 L. Gu, N. Y. Cui, L. Cheng, Q. Xu, S. Bai, M. M. Yuan, W. W. Wu, J. M. Liu, Y. Zhao, F. Ma, Y. Qin and Z. L. Wang, *Nano Lett.*, 2013, **13**, 91–94.
- 34 F. Zhang, C. Z. Yuan, J. J. Zhu, J. Wang, X. G. Zhang and X. W. Lou, *Adv. Funct. Mater.*, 2013, **23**, 3909–3915.
- 35 H. O. Pierson, *Handbook of Carbon, Graphite, Diamond, and Fullerenes: Properties, Processing, and Applications*, Noyes Publications, 1993.
- 36 Q. H. Guo, X. P. Zhou, X. Y. Li, S. L. Chen, A. Seema, A. Greiner and H. Q. Hou, *J. Mater. Chem.*, 2009, **19**, 2810–2816.
- 37 Y. Wang, J. G. Tang, S. Q. Xie, J. X. Liu, Z. C. Xin, X. L. Liu and L. A. Belfiore, *RSC Adv.*, 2015, **5**, 42174–42177.
- 38 W. S. Hummers and R. E. Offeman, *J. Am. Chem. Soc.*, 1958, **80**, 1339–1339.
- 39 Y. P. Huang, Y. E. Miao, J. Fu, S. Y. Mo, C. Wei and T. X. Liu, *J. Mater. Chem. A*, 2015, **3**, 16263–16271.
- 40 M. S. Faber, R. Dziejczak, M. A. Lukowski, N. S. Kaiser, Q. Ding and S. Jin, *J. Am. Chem. Soc.*, 2014, **136**, 10053–10061.
- 41 J. Mittal, O. P. Bahl, R. B. Mathur and N. K. Sandle, *Carbon*, 1994, **32**, 1133–1136.
- 42 X. G. Mei and J. Y. Ouyang, *Carbon*, 2011, **49**, 5389–5397.
- 43 S. S. Ji, Z. Yang, C. Zhang, Z. Y. Liu, W. W. Tjiu, I. Y. Phang, Z. Zhang, J. S. Pan and T. X. Liu, *Electrochim. Acta*, 2013, **109**, 269–275.
- 44 M. A. Lukowski, A. S. Daniel, F. Meng, A. Forticaux, L. S. Li and S. Jin, *J. Am. Chem. Soc.*, 2013, **135**, 10274–10277.
- 45 C. Xu, S. J. Peng, C. L. Tan, H. X. Ang, H. T. Tan, H. Zhang and Q. Y. Yan, *J. Mater. Chem. A*, 2014, **2**, 5597–5601.
- 46 H. Tang, K. P. Dou, C. C. Kaun, Q. Kuang and S. H. Yang, *J. Mater. Chem. A*, 2014, **2**, 360–364.
- 47 H. Vruble and X. L. Hu, *Angew. Chem., Int. Ed.*, 2012, **124**, 12875–12878.
- 48 X. X. Zou, X. X. Huang, A. Goswami, R. Silva, B. R. Sathe, E. Mikmeková and T. Asefa, *Angew. Chem., Int. Ed.*, 2014, **126**, 4461–4465.
- 49 J. Q. Tian, Q. Liu, A. M. Asiri and X. P. Sun, *J. Am. Chem. Soc.*, 2014, **136**, 7587–7590.